Defense Technical Information Center
Compilation Part Notice

ADP011849

TITLE: Exit Pupil Patterns from Optical Disks

DISTRIBUTION: Approved for public release, distribution unlimited

This paper is part of the following report:

TITLE: Optical Storage and Optical Information Held in Taipei, Taiwan on 26-27 July 2000

To order the complete compilation report, use: ADA399082

The component part is provided here to allow users access to individually authored sections of proceedings, annals, symposia, etc. However, the component should be considered within the context of the overall compilation report and not as a stand-alone technical report.

The following component part numbers comprise the compilation report:
ADP011833 thru ADP011864

Exit Pupil Patterns from Optical Disks

Robert S. Upton and Tom D. Milster

Optical Sciences Center, University of Arizona, Tucson, AZ, USA, 85721

ABSTRACT

The modulation of the irradiance in the exit pupil of an optical data storage scanning system is described by analyzing the behavior of scan-dependent interference fringes. These fringes are grouped into three independent irradiance components. The variation of the exit pupil irradiance pattern as a function of groove depth is discussed.

Keywords: Diffraction, Interference, Pupil Irradiance Modulation, Scanning Optical Microscope

1. INTRODUCTION

Optical data storage scanning systems are a sub-class of optical microscopes that use a coherent laser source. The laser light is focused onto semi-periodic marks recorded on the data layer of a rotating optical disk. The semi-periodic property of the marks the marks to be well represented by a Fourier series. The laser light field scattered from the optical disk is collected by a high numerical aperture (high-NA) collection lens. The electronic readout signal is generated by a detector placed in the exit pupil. In this paper, the effects of the phase depth of the pre-grooves on the disk on the exit pupil irradiance modulation are discussed. The exit pupil irradiance modulation with varying groove depth is simulated using Optiscan,[1] which is a Matlab[2] based diffraction code.

Section 2.1 presents a high-NA scalar diffraction model that is used to describe the propgation of the light fields from the optical disk to the exit pupil.[3] Section 2.2 also presents a technique that describes the reflected light field from the optical disk as a linear summation of component disk fields by Babinet's principle.[4] Section 3 presents the simulation parameters and optical disk model used in the computer simulations. Section 4 presents the simulated exit pupil irradiance modulations.

2. DIFFRACTION MODEL

In this section a high-NA scalar diffraction theory is outlined and the linear decomposition of the light field reflected from the optical disk is discussed.

2.1. High NA Scalar Diffraction Theory

Figure 1 shows a simplified layout of the optical data storage scanning system. Light from the laser source is collimated and then focused onto the optical disk where it interacts with the data marks. The data marks scatter the incident laser light, which is collected by the collection lens. The scanning system can be represented by the illumination pupil, disk and collection pupil, as shown in Fig. 1(b).

The light field in the illumination pupil is denoted by $\tilde{O}_{ILL}(\alpha, \beta)$. α and β are direction cosines, which are also the coordinates of the pupils. The focused light field on the optical disk is denoted by $O_{DISK}(\hat{x}, \hat{y})$. $\hat{x}$ and $\hat{y}$ are wavelength-normalized spatial variables. The relationship between the direction cosines and the wavelength-normalized variables is described by a propagating plane wave,

$$U(\hat{x}, \hat{y}) = A(\hat{x}, \hat{y}) \exp[2\pi i(\hat{x}\alpha + \hat{y}\beta)]. \tag{1}$$

α and β are also Fourier transform conjugate[5,6] variables with $\hat{x}$ and $\hat{y}$, respectively.

The relationship between $\tilde{O}_{ILL}(\alpha, \beta)$ and $O_{DISK}(\hat{x}, \hat{y})$ is,

$$O_{DISK}(\hat{x}, \hat{y}) = \exp\left[-\pi i \left(\frac{\hat{x}^2 + \hat{y}^2}{\hat{r}}\right)\right] \int_{\infty}^{\infty} \int_{\infty}^{\infty} \tilde{O}_{ILL}(\alpha, \beta) \frac{\hat{r} \exp(-i2\pi\hat{r})}{i\gamma} \exp[2\pi i(\alpha\hat{x} + \beta\hat{y})] d\alpha d\beta, \tag{2}$$

Further author information: (Send correspondence to Tom D. Milster)
Robert S. Upton: E-mail: rsupton@u.arizona.edu
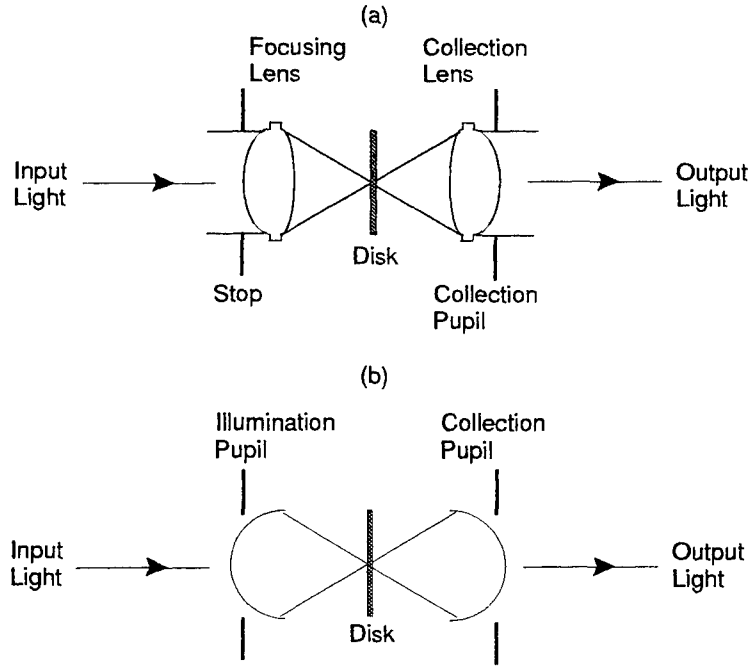Tom D. Milster: E-mail: milster@arizona.edu

Figure 1. A schematic showing the geometry of an optical data storage scanning system. (a) The optical data storage scanning system is shown unfolded. (b) The scanning system can be represented as an illumination pupil, optical disk and collection pupil. The fields in the pupils reside on a surface called the reference sphere. The radius of the reference sphere in the illumination pupil equal to the radius of the focusing light field and the radius of the reference sphere in the collection pupil equal to the radius of the diffracted light field.

where $\hat{r}$ is the wavelength-normalized radius of the illumination pupil illustrated in Fig 1(b).

$O_{DISK}(\hat{x}, \hat{y})$ is modified upon reflection by the data marks, which are represented by the mark reflectivity function $C_R(\hat{x}, \hat{y})$. The field reflected from the disk is,

$$U_{DISK} = C_R(\hat{x}, \hat{y})O_{DISK}(\hat{x}, \hat{y}). \tag{3}$$

The form of the reflected field in the collection pupil, $\tilde{O}_{COLL}(\alpha, \beta)$ is,

$$\tilde{O}_{COLL}(\alpha, \beta) = \int_{\infty}^{\infty} \int_{\infty}^{\infty} U_{DISK}(\hat{x}, \hat{y}) \left[\frac{i\gamma \exp{(i2\pi\hat{r})}}{\hat{r}} \exp{\left[\pi i \left(\frac{\hat{x}^2 + \hat{y}^2}{\hat{r}}\right)\right]} \right] \exp{\left[-2\pi i(\alpha\hat{x} + \beta\hat{y})\right]} d\alpha d\beta. \tag{4}$$

Substitution of Eq. (4) into Eq. (2) and use of the convolution theorem for Fourier transforms[7] results in a simple analytical expression for $\tilde{O}_{COLL}(\alpha, \beta)$, which is,

$$\tilde{O}_{COLL}(\alpha, \beta) = \int_{\infty}^{\infty} \int_{\infty}^{\infty} \tilde{O}_{ILL}(\alpha', \beta')\tilde{C}_R(\alpha - \alpha', \beta - \beta') d\alpha' d\beta'. \tag{5}$$

$\tilde{C}_R(\alpha, \beta)$ is the Fourier transform of the mark reflectivity function. Therefore, the field in the collection pupil is the two-dimensional convolution between the Fourier transform of the disk reflectivity function and the field in the illumination pupil.

The irradiance in the collection pupil, $\tilde{E}_{COLL}(\alpha, \beta)$ is

$$\tilde{E}_{COLL}(\alpha, \beta) = \tilde{O}_{COLL}(\alpha', \beta')^* \tilde{O}_{COLL}(\alpha, \beta). \tag{6}$$

2.2. Linear Decomposition of the Optical Disk Light Field

This section is a mathematical description of the exit pupil irradiance modulation using the scalar diffraction model developed in section 2.1.
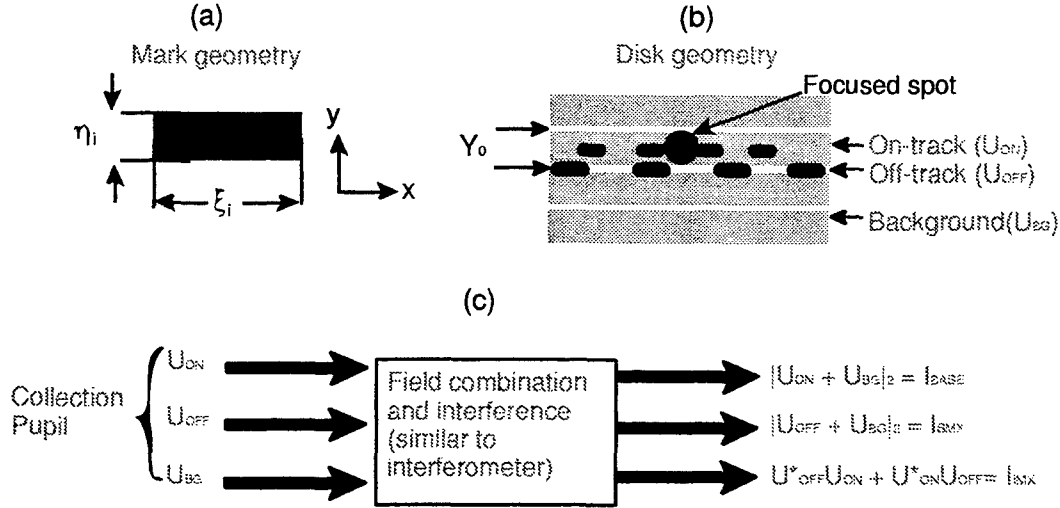

Figure 2. A schematic showing the disk model used in the formation of the exit pupil irradiance. (a) The mark geometry and shape simulated. ξ_i and η_i are the length and width of the data mark on the i'th data track. (b) The disk geometry and disk component fields for on-track, U_{ON}, off-track, U_{OFF}, and background, U_{BG}, are shown. (c) The fields in the pupil combine and form the pupil irradiance. The total pupil irradiance is decomposed into three signal groups. The first group is BASE, which is the combination of U_{ON} and U_{BG}. The second signal group is SMX, which is the combination of U_{OFF} and U_{BG}. The third group is IMX, which the interference between U_{ON} and U_{OFF}.

In this section the total field reflected from the disk, $U_{DISK}(\hat{x}, \hat{y})$, is re-expressed as a linear combination of disk component fields by use of Babinet's principle.[4,8] The disk component fields are also known as the Babinet fields. Figure 2 is a schematic of the disk model used in the description of the diffraction from the optical disk to the collection pupil. The total field reflected from the optical disk is rewritten as,

$$U_{DISK}(\hat{x}, \hat{y}) = [r_L u_{BG}(\hat{x}, \hat{y}) + (r_M - r_L)u_{ON}(\hat{x}, \hat{y}) + \exp(i\phi_G)(r_M - r_L)u_{OFF}(\hat{x}, \hat{y})]\,O_{DISK}(\hat{x}, \hat{y}). \qquad (7)$$

$|r_L|$ is the scalar reflectivity of the disk without data marks, $|r_M|$ is the scalar reflectivity of the data marks and ϕ_G is the phase depth of the pre-grooves on the disk. ϕ_G is related to the physical groove depth d by,

$$\phi_G = \frac{4\pi d}{\lambda}, \qquad (8)$$

where λ is the vacuum wavelength of the light source. The off-track data marks are located in a groove, therefore the phase of $u_{OFF}(\hat{x}, \hat{y})$ is modified by ϕ_G.

One of the properties of optical data storage scanning systems are semi-periodic data marks. The semi-periodic property of the data marks allows the Babinet fields, $u_{ON}(\hat{x}, \hat{y})$, $u_{OFF}(\hat{x}, \hat{y})$ and $u_{BG}(\hat{x}, \hat{y})$, to be expressed as a Fourier series.[5,9,7] Therefore, using the parameters defined in Fig. 2(a) and (b), $u_{ON}(\hat{x}, \hat{y})$, $u_{OFF}(\hat{x}, \hat{y})$ and $u_{BG}(\hat{x}, \hat{y})$ are

$$u_{ON}(\hat{x}, \hat{y}) = f_1(\hat{y}) \sum_{m=-M}^{M} R_m \exp\left[-2\pi i m\left(\frac{\hat{x}_0 - \hat{x}}{T_1}\right)\right] \star \delta(\hat{y}), \qquad (9)$$

$$u_{OFF}(\hat{x}, \hat{y}) = f_2(\hat{y}) \sum_{m=-M}^{M} S_m \exp[-2\pi i m \left(\frac{\hat{x}_0' - \hat{x}}{T_2}\right)] \star \delta(\hat{y} - \hat{Y}_0), \tag{10}$$

$$u_{BG}(\hat{x}, \hat{y}) = \sum_{n=-N}^{N} A_n \exp[2\pi i n \left(\frac{\hat{y}}{Y_0}\right)]. \tag{11}$$

In our analysis, the data marks are separable functions of x and y, which allows the pupil fields associated with the marks to be represented as separable functions of α and β. The delta functions $\delta(\hat{y})$ and $\delta(\hat{y} - \hat{y}_0)$ in Eqs. 9 and 10 locate the y center of the data tracks. Therefore u_{ON} and u_{OFF} have their y centers located at $y = 0$ and $y = y_0$, respectively. The functions $f_1(\hat{y})$ and $f_2(\hat{y})$ describe the variation of $u_{ON}(\hat{x}, \hat{y})$ and $u_{OFF}(\hat{x}, \hat{y})$ along the y direction. The $\star$ describes a one dimensional convolution operation. R_m, S_m and A_n are the Fourier weighting coefficients. The coefficients are dependent upon the mark shape and size.

The corresponding Babinet fields in the collection pupil are calculated by taking the Fourier transforms of Eqs. 9, 10 and 11, and then applying Eq. 5. The result is,

$$\tilde{O}_{ON}(\alpha, \beta) = \sum_{m=-M}^{M} R_m \exp[-2\pi i m \left(\frac{\hat{x}_0}{\hat{T}_1}\right)][F_1(\beta) \star \tilde{O}_{ILL}(\alpha - \frac{m}{\hat{T}_1}, \beta)], \tag{12}$$

$$\tilde{O}_{OFF}(\alpha, \beta) = \sum_{m=-M}^{M} S_m \exp[-2\pi i m \left(\frac{\hat{x}_0' - \hat{x}}{T_2}\right)][F_2(\beta) \exp(-2\pi i \beta \hat{y}_0) \star \tilde{O}_{ILL}(\alpha - \frac{m}{\hat{T}_1}, \beta)], \tag{13}$$

$$\tilde{O}_{BG}(\alpha, \beta) = \tilde{O}_{ILL}(\alpha, \beta) + [\exp(i\phi_G) - 1] \sum_{n=-N}^{N} A_n \tilde{O}_{ILL}(\alpha, \beta - \frac{n}{\hat{y}_0}). \tag{14}$$

$\tilde{O}_{OFF}(\alpha, \beta)$ in Eq. 13 contains a linear phase in the beta direction of the pupil due to the off-set of $u_{OFF}(\hat{x}, \hat{y})$ from the on-track. The functions $F_1(\beta)$ and $F_2(\beta)$ are Fourier transforms of the functions $f_1(\hat{y})$ and $f_2(\hat{y})$, respectively. The one-dimensional convolution functions in Eqs. 12 and 13 can be represented as a single function, κ_m,

$$[F_1(\beta) \star \tilde{O}_{ILL}(\alpha - \frac{m}{\hat{T}_1}, \beta)] = \kappa_m(\beta, 0) \tag{15}$$

$$[F_2(\beta) \exp(-2\pi i \beta \hat{y}_0) \star \tilde{O}_{ILL}(\alpha - \frac{m}{\hat{T}_1}, \beta)] = \kappa_m(\beta, \hat{y}_0). \tag{16}$$

$\kappa_m(\beta, \hat{y}_0)$ is a complex number and $\kappa_m(\beta, 0)$ corresponds to the case $\hat{y}_0 = 0$. Figure 3 shows the amplitude and phase variation of κ_m along the β direction of the pupil for the on-track case and the off-track case. In Fig. 3(a) the amplitude of the off-track field in the pupil is smaller than the on-track amplitude as a consequence of the linear phase component of $\kappa_m(\beta, \hat{y}_0)$ in Eq. 16. In Fig. 3(b) the linear phase in Eq. 16 results in a linearly varying phase along the β direction for the off-track scanning case. From Eqs. 12, 13 and 14 the Babinet fields in the pupil are distributed into a summation of diffraction orders. The diffraction orders in Eqs. 12 and 13 are distributed in the α direction, which is in the scan-direction of the pupil. This distribution occurs because $u_{ON}(\alpha, \beta)$ and $u_{OFF}(\alpha, \beta)$ are arranged in the scan direction of the disk. This distribution is illustrated in Fig. 4.

The total field in the collection pupil, $\tilde{O}_{COLL}$ is written as,

$$\tilde{O}_{COLL} = r_L \tilde{O}_{BG} + (r_M - r_L) \exp(i\phi_G) \tilde{O}_{ON} + (r_M - r_L) \tilde{O}_{OFF}. \tag{17}$$

The irradiance in the pupil is calculated by means of Eq. 6. The irradiance in the pupil is described by a summation of interference fringes, some of which modulate the irradiance pattern as the marks are scanned. The modulating fringes in the pupil are grouped into the three signal groups, $E_{BASE}(\alpha, \beta; \hat{x}_0)$, $E_{SMX}(\alpha, \beta; \hat{x}_0)$ and $E_{IMX}(\alpha, \beta; \hat{x}_0)$, as described in Fig. 2. The explicit form of the BASE signal group is,

$$\begin{aligned} E_{BASE}(\alpha, \beta; \hat{x}_0) = \ & 2\Delta r^2 \sum_m R_m^2 |\kappa(\beta; 0)|^2 \left[\cos\left(2\pi m \frac{\hat{x}_0}{\hat{T}_1}\right) + \sin\left(2\pi m \frac{\hat{x}_0}{\hat{T}_1}\right)\right] \\ & + 2r_L \Delta r \sum_m R_m \kappa_m(\beta; 0) \tilde{O}_{ILL}(\alpha, \beta) \cos\left(2\pi m \frac{\hat{x}_0}{\hat{T}_1}\right) \\ & + 2r_L \Delta r \sum_m \sum_n R_m A_n \kappa_m(\beta; 0) \left[\cos\left(2\pi m \frac{\hat{x}_0}{\hat{T}_1} + \phi_G\right) - \cos\left(2\pi m \frac{\hat{x}_0}{\hat{T}_1}\right)\right] \tilde{O}_{ILL}(\alpha, \beta - \frac{n}{\hat{y}_0}). \end{aligned} \tag{18}$$
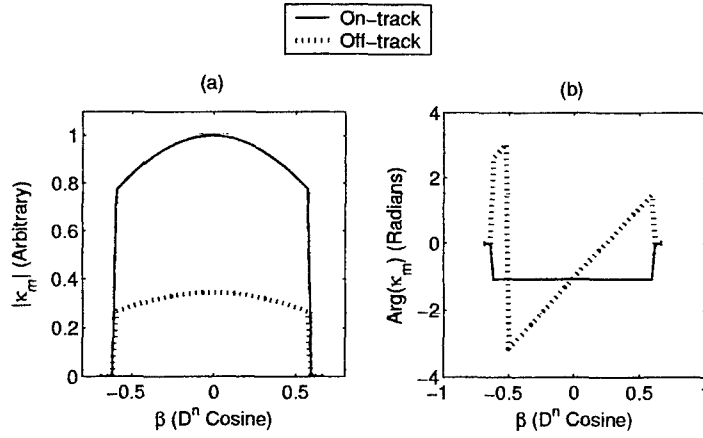
146

Figure 3. The variation of the **(a)** amplitude and **(b)** phase of the one-dimensional convolution along β for on-track and off-track scanning that is represented by $|\kappa_m|$ and $Arg(\kappa_m)$, respectively.
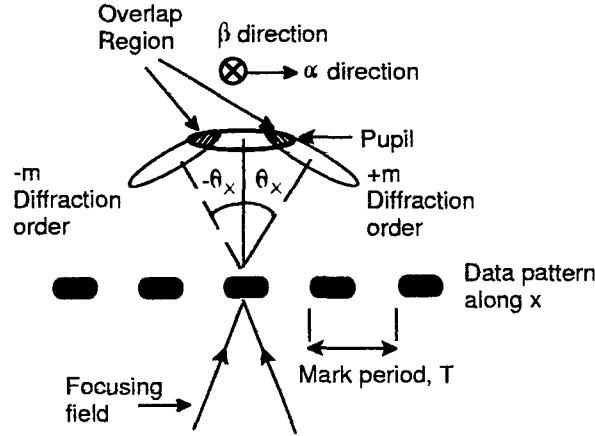

Figure 4. For periodic marks arranged along the x direction of the disk the diffraction orders are arranged along α in the pupil. The modulation of the irradiance in the pupil occurs in the overlap regions between the different scan-track higher diffraction orders ($\hat{O}_{ON}$ and $\hat{O}_{OFF}$), and the diffraction orders of $\hat{O}_{BG}(\alpha,\beta)$.

$E_{BASE}(\alpha, \beta; \hat{x}_0)$ consists of three distinct sets of interference fringes. The first set is the interference of the higher m on-track diffraction orders. The phase of the modulation of this fringe has cos and sin components, which are in quadrature with respect to each other.

The explicit form of the SMX signal group is,

$$
\begin{aligned}
E_{SMX}(\alpha,\beta;\hat{x}_0) \;=\; & 2\Delta r^2 \sum_m S_m^2 |\kappa(\beta;\hat{y}_0)|^2 \left[\cos\left(2\pi m \frac{\hat{x}_0'}{\hat{T}_2} + Arg(\kappa_m)\right) + \sin\left(2\pi m \frac{\hat{x}_0'}{\hat{T}_2} + Arg(\kappa_m)\right) \right] \quad (19) \\
& + 2r_L \Delta r \sum_m S_m \kappa_m(\beta;\hat{y}_0) \tilde{O}_{ILL}(\alpha,\beta) \cos\left(2\pi m \frac{\hat{x}_0'}{\hat{T}_2} + Arg(\kappa_m) - \phi_G\right) \\
& + 2r_L \Delta r \sum_m \sum_n S_m A_n \kappa_m(\beta;\hat{y}_0) \cos\left(2\pi m \frac{\hat{x}_0'}{\hat{T}_2} + Arg(\kappa_m)\right) \tilde{O}_{ILL}(\alpha, \beta - \frac{n}{\hat{y}_0})
\end{aligned}
$$

$$- \quad 2r_L \Delta r \sum_m \sum_n S_m A_n \kappa_m(\beta; \hat{y}_0) \cos\left(2\pi m \frac{\hat{x}_0'}{\hat{T}_2} + Arg(\kappa_m) - \phi_G\right) \tilde{O}_{ILL}(\alpha, \beta - \frac{n}{\hat{y}_0}).$$

Like $E_{BASE}(\alpha, \beta, \hat{x}_0)$, $E_{SMX}(\alpha, \beta, \hat{x}_0)$ has three distinct sets of interference fringes. The first set is a result of the interference between the off-track pupil fields. From Fig.3(b) $Arg(\kappa_m)$ is a linearly varying phase function with respect to β. $Arg(\kappa) < 0$ for $-NA < \beta < 0$ and $Arg(\kappa) > 0$ for $0 < \beta < NA$. The effect of $Arg(\kappa_m)$ combined with the scan phase, $2\pi m \hat{x}_0 / \hat{T}_2$, is described with the aid of Fig. 5. The phases in the four quadrants are,

$$\phi_A = Arg(\kappa_m) - 2\pi m \frac{\hat{x}_0}{\hat{T}_2}, \tag{20}$$

$$\phi_B = -Arg(\kappa_m) - 2\pi m \frac{\hat{x}_0}{\hat{T}_2}, \tag{21}$$

$$\phi_C = -Arg(\kappa_m) + 2\pi m \frac{\hat{x}_0}{\hat{T}_2}, \tag{22}$$

$$\phi_D = Arg(\kappa_m) + 2\pi m \frac{\hat{x}_0}{\hat{T}_2}. \tag{23}$$

Taking the cos and sin values of the phases describes the modulation between the four quadrants that is rotational. The modulation of the remaining sets of fringes is also rotational due to a similar phase variation between the four quadrants. The presence of ϕ_G in the phases of these fringes results in a shift of these fringes along the β direction of the pupil. The shift of these fringes affects the overall rotation modulation of $E_{SMX}(\alpha, \beta, \hat{x}_0)$ in the pupil. This is further described in sections 4.2 and 4.3. The rotational characteristic of the exit pupil irradiance as off-track marks are scanned is the basis of segmented pupil detection schemes for tracking[10] and crosstalk cancellation[11,12] in optical data storage. The rotation of the exit pupil irradiance for off-track scanning can be quantified by quadrant pupil detection,[10,11] in which the detector in the exit pupil is divided into quadrants, as in Fig. 5. Taking the sums of the integrated irradiance along the two diagonals and then taking their difference results in the QPD signal $i_{QPD}(t)$. Mathematically this is

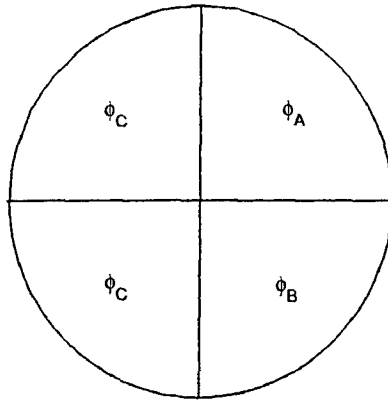$$i_{QPD} = i_A + i_C - i_B - i_D. \tag{24}$$

Figure 5. The modulation of $E_{SMX}(\alpha, \beta, \hat{x}_0)$ in the pupil can be described by considering the phase of the cos and sin modulation in four quadrants of the pupil. The phases of the modulations in the four quadrants is denoted by ϕ_A, ϕ_B, ϕ_C and ϕ_D, respectively. The rotational modulation of $E_{SMX}(\alpha, \beta, \hat{x}_0)$ is quantified by the quadrant pupil detection signal, which is $i_{QPD} = i_A + i_C - i_B - i_D$.

The form of the $E_{IMX}(\alpha, \beta, \hat{x}_0)$ is,

$$E_{IMX}(\alpha, \beta; t) = 2\Delta r^2 \sum_m R_m S_m |\kappa_m(\beta; 0)\kappa_m(\beta; \hat{y}_0)| \cos\left[2\pi m \left(\frac{\hat{x}_0'}{\hat{T}_2} - \frac{\hat{x}_0}{\hat{T}_1}\right) - Arg(\kappa_m) - \phi_G\right]. \tag{25}$$

$E_{IMX}(\alpha, \beta, \hat{x}_0)$ consists of a single set of fringes. As with $E_{SMX}(\alpha, \beta, \hat{x}_0)$ in Eq. 19 the IMX interference fringe has rotational characteristics due to the linear property of $Arg(\kappa_m)$ in the phase of the fringe modulation. The presence of ϕ_G in the interference fringe causes the IMX fringe to be shifted in the pupil for different groove depths.

3. DISK MODEL AND SIMULATION PARAMETERS

Table 1 lists the simulation parameters for the quantities described in Fig. 2. The simulation parameters also include the the disk reflectivities and the variation of groove depth. These parameters are programed in Optiscan and the signal groups are calculated according to the linear decomposition model developed in section 2.2.

Table 1. The simulation parameters for the disk model. The quantities listed refer to the parameters given in Fig 2.

λ	0.65μm
NA	0.6
y_0	0.5μm
Groove Depths	0, $\lambda/40$, $\lambda/20$ $3\lambda/40$, $\lambda/10$, $\lambda/8$, $6\lambda/40$, $7\lambda/40$, $\lambda/5$, $9\lambda/40$, $\lambda/4$
η	$0.4\mu m$
ξ_1	$1.08\mu m$
ξ_2	$1.08\mu m$
r_M	0.006
r_L	0.2

4. THE IRRADIANCE MODULATION IN THE COLLECTION PUPIL

This section presents simulated exit pupil irradiance modulation results. The results are separated into three sections containing the BASE, SMX and IMX pupil irradiances, respectively. The pupil irradiances for each signal group are shown for the four scan locations, I, II, III, IV, which are shown in Fig. 6.
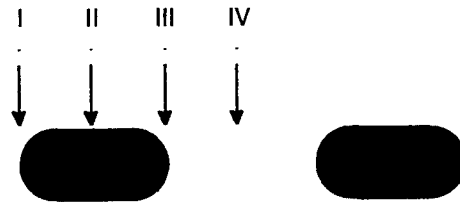

Figure 6. The scan locations, I, II, III, IV on the disk corresponding to the pupil irradiances shown in sections 4.1, 4.2 and 4.3.

4.1. The On-track Data Irradiance Modulation (BASE)

Figure 7 shows the the on-track scanning pupil irradiances for for the scan positions and groove depths indicated. The diffraction orders introduced by the grooved background are clearly seen lying along the β direction of the pupil for groove depths greater than zero.

The modulation of the fringes is along the α direction of the pupil. The data marks being scanned lie along the x direction of the disk, introducing the higher on-track diffraction orders in the α direction of the pupil, which is illustrated in Fig. 4. The modulation along α occurs from the overlap of the higher on-track diffraction orders with the on-track zero'th order and background fields. The symmetry of the fringe modulation along α is determined by

the groove depth. This can be seen from the variation of the pupil irradiance patterns for changing groove depths for scan position I. The effect of groove depth on the pupil irradiances leads to the conclusion that the modulating fringe that contains the phase of the groove in the cosine dominates the BASE signal group modulation for groove depths greater than zero. The fringe in question is described by the third term in Eq. 18, which is,

$$2r_L \Delta r \sum_m \sum_n R_m A_n \kappa_m(\beta;0) \left[\cos\left(2\pi m \frac{\hat{x}_0}{\hat{T}_1} + \phi_G \right) - \cos\left(2\pi m \frac{\hat{x}_0}{\hat{T}_1} \right) \right] \tilde{O}_{ILL}(\alpha, \beta - \frac{n}{\hat{y}_0}). \tag{26}$$
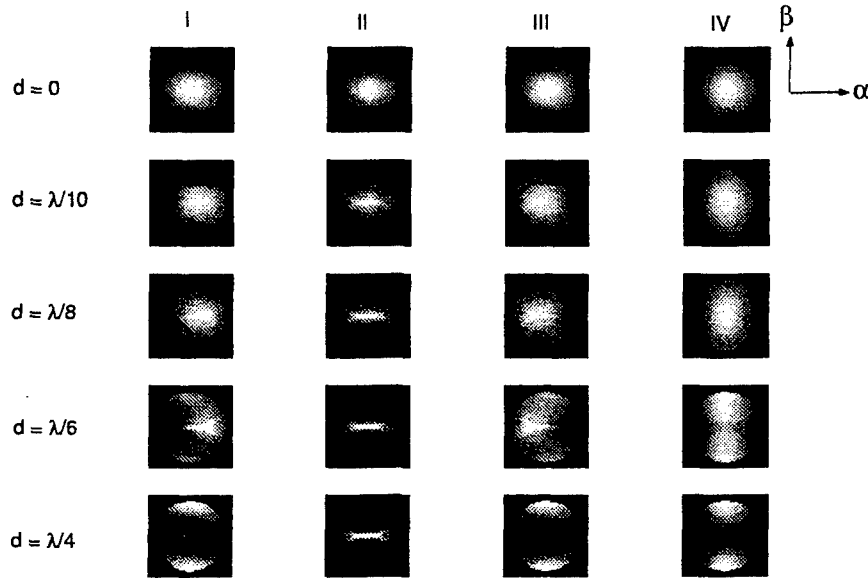

Figure 7. The pupil irradiance modulation for the BASE signal group. The pupil patterns are arranged for the groove depths indicated in rows and in columns for the scan positions I, II, III and IV. The bright portions of the pupil are positive contributions to the pupil irradiance and the dark portions are zero.

The form of Eq. 26 can be used to predict the symmetry of the fringe movement along the α direction of the pupil. Fig. 8 is a cosine function describing the BASE irradiance modulation between the $\alpha > 0$ and $\alpha < 0$ portions of the pupil. For $\phi_G = 0$, which corresponds to position A on the cosine function in Fig. 8, the modulation of the fringe in the pupil, described by Eq. 26, is the same for $\alpha > 0$ and $\alpha < 0$. For $\lambda/8$ groove depth, which corresponds to position B on the cosine function, the modulation of the fringe in the pupil for $\alpha > 0$ has opposite phase to the modulation of the fringe in the $\alpha < 0$ portion of the pupil. Therefore, according to Eq. 26 the difference of the integrated irradiance between the $\alpha > 0$ portion and the $\alpha < 0$ portion is a maximum for groove depth of $\lambda/8$. This is confirmed by the results of the computer simulation, as shown in Fig. 9.

4.2. The Off-track Data Irradiance Modulation (SMX)

Figure 10 shows the off-track scanning pupil irradiances for the groove depths and scan locations indicated. The scan locations, I, II, III and IV are shown in Fig. 6. The bright portions of the pupil are positive contributions to the irradiance and the dark portions are zero. The modulation of the irradiance in the pupil is highly dependent upon groove depth. This is seen from the plots in Fig. 11(a) and (b).

All the modulating fringes in Eq. 19 rotate as the off-track data marks on the disk are scanned. For the groove depth of zero the modulation of the irradiance is determined by one set of fringes, which is highly rotational, as can be seen by the large QPD amplitude in Fig. 11(a). By introducing a grooved substrate, more interference fringes are introduced into the pupil. This effect is seen from Eq. 19. Each of the fringes has a rotational modulation in the pupil, but the groove dependent fringes are shifted in the pupil by an amount that is determined by the value of ϕ_G.
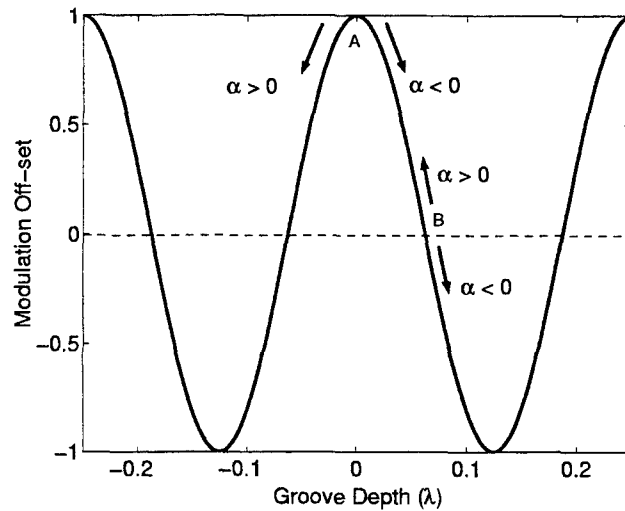
Figure 8. The modulation of the BASE signal group fringe can be described by considering the fringe modulation off-set values, which are dependent upon the groove depth. Positions A and B on the cosine function correspond to groove depths 0 and $\lambda/8$, respectively. The arrows correspond to modulation of the fringe for the $\alpha > 0$ and $\alpha < 0$ portions of the pupil.
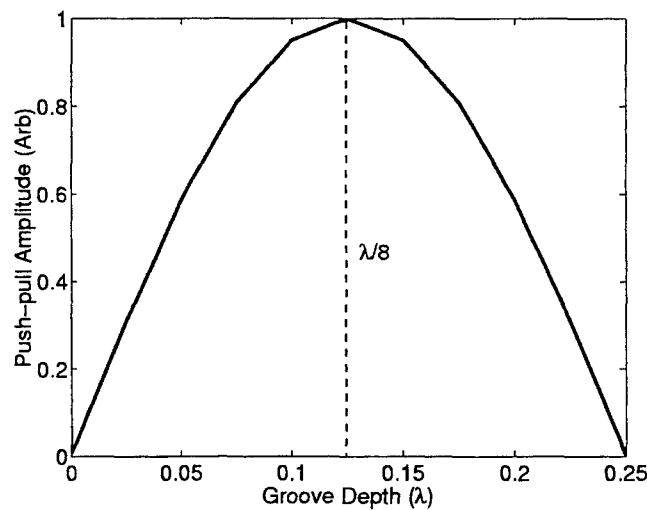

Figure 9. The amplitude of the integrated irradiance modulation for the BASE signal group between the $\alpha > 0$ and $\alpha < 0$ portions of the pupil.

This shift has the effect of reducing the overall rotation of the total irradiance, and increasing the modulation along the β direction of the pupil. The amplitude of the modulation of the fringes along the β direction of the pupil for different groove depths can be seen in Fig. 11(b). For the range of groove depths $\lambda/10 < d < \lambda/6$ the modulation of fringes is almost exclusively along the β direction of the pupil, with very little rotation.

4.3. The Irradiance Modulation of the Interference between On-track and Off-track (IMX)

Figure 12 shows pupil irradiances for the interference between the on-track and off-track fields. The bright regions are positive contributions to the irradiance and the dark regions of are negative contributions to the irradiance. This
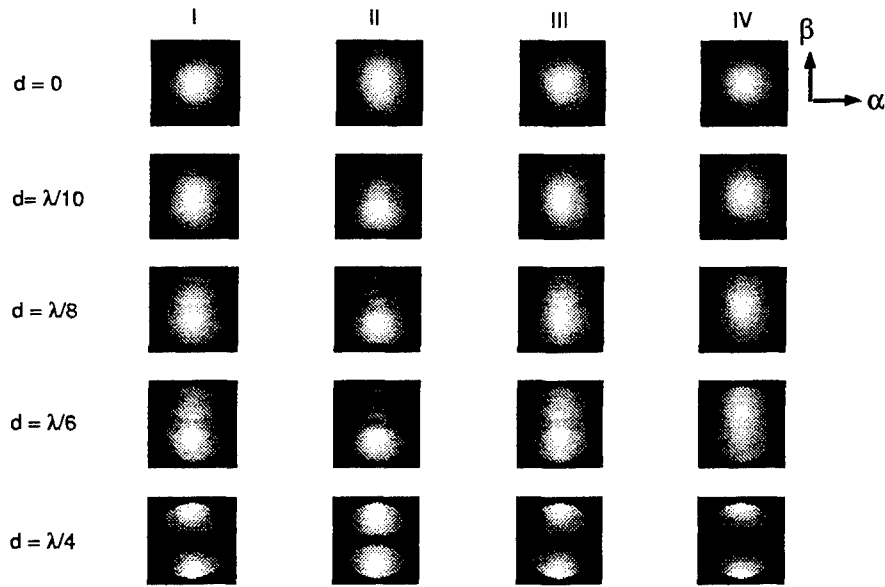
Figure 10. The pupil irradiance modulation for the SMX signal group. The pupil patterns are arranged for the groove depths indicated in rows and in columns for the scan positions I, II, III and IV. The bright portions of the pupil are positive contributions to the irradiance and the dark portions of the pupil are zero.
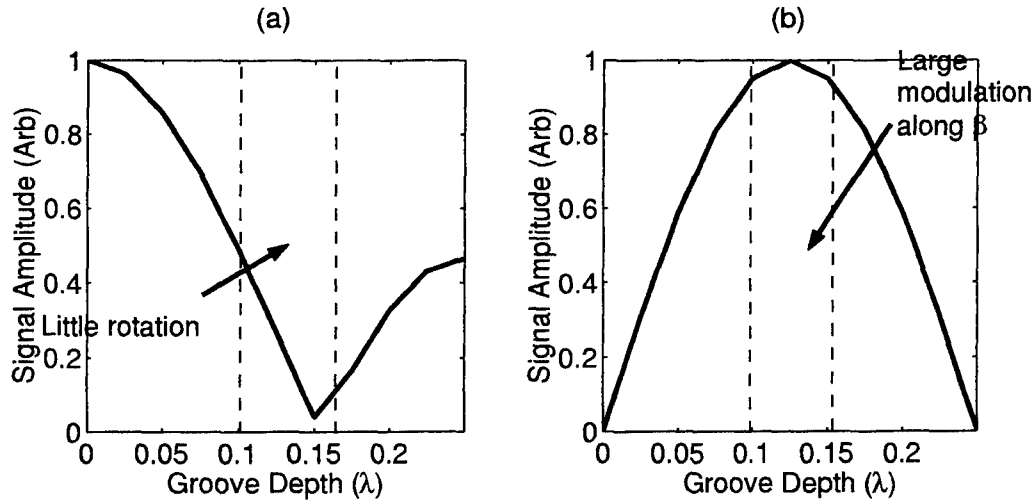

Figure 11. For the SMX signal group. (a) The amplitude of the QPD signal as a function of groove depth. (b) The amplitude of the integrated irradiance between the $\beta > 0$ and $\beta < 0$ portions of the pupil.

is a result of the IMX signal group being a cross modulation between the on-track and off-track fields. Eq. 25 shows that the IMX pupil irradiance consists of a single set of fringes. The modulation of the IMX fringe in the pupil is highly rotational. IMX is more rotational for all groove depths compared with SMX because IMX consists of a single interference fringe.

The IMX fringe shifts along the β direction of the pupil for differing groove depths. The rotation of the fringe is unaffected by the groove depth. However, the shifting IMX fringe affects the integrated readout signal. This is due
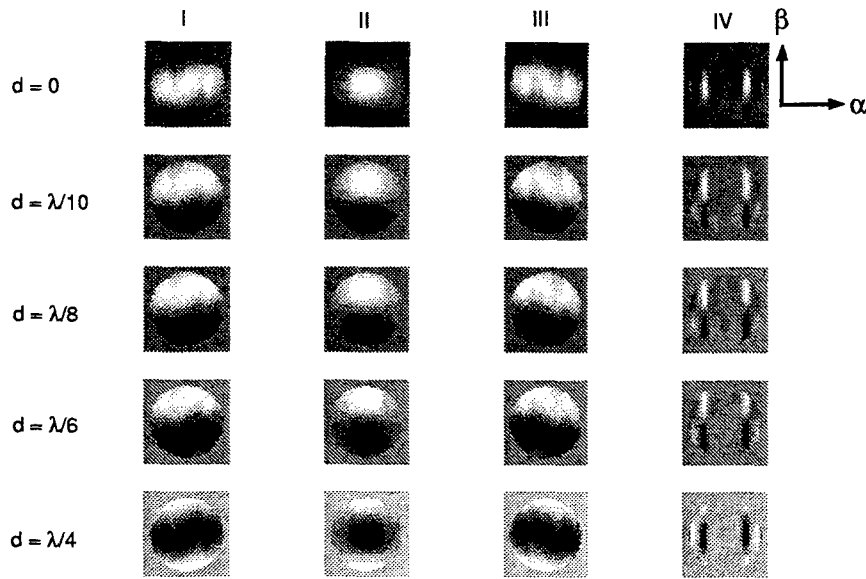
Figure 12. The pupil irradiance modulation for the IMX signal group. The pupil patterns are arranged for the groove depths indicated in rows and in columns for the scan positions I, II, III and IV. The bright portions of the pupil are positive contributions to IMX irradiance and the dark portions of the pupil are negative contributions.

to the distribution of the IMX fringe in the pupil. For groove depth $\lambda/8$ there are equal amounts of positive and negative irradiance contributions in the pupil, which gives an integrated signal of zero. The same occurs for forming the QPD signal, as shown in Fig. 13.

5. CONCLUSIONS

The total field reflected from the optical disk is described as a linear summation of fields reflected from the on-track data marks, off-track data marks and the background, respectively. The fields are propagated to the exit pupil of the optical data storage scanning system where they combine and interfere to form the total exit pupil irradiance pattern. The total exit pupil irradiance is grouped into three meaningful terms, BASE, SMX and IMX. The BASE irradiance results from the combination of the on-track field with the background field. The SMX irradiance results from the combination of the off-track fields with the background fields. The IMX irradiance occurs as a result of the interference between the on-track fields and the off-track fields. The modulating components of BASE, SMX and IMX are termed the BASE, SMX and IMX signal groups.

The modulation of the pupil irradiances for the signal groups is described by the modulation of interference fringes. The BASE and SMX signal groups consist of three groups of interference fringes. The IMX signal group consists of a single group of interference fringes. The BASE signal group modulates along the α direction of the pupil, which is also the scan-track direction. The symmetry of the movement along α is affected by the interference fringes whose modulation is explicitly dependent upon the groove depth.

The modulation of the SMX and IMX signal groups is largely rotational. The rotation of the irradiance is a consequence of the linear dependence in phase along the β direction of the pupil of the fields diffracted from the off-track marks combined with the phase of the higher diffraction orders along the α direction of the pupil changing linearly with scan location. However, for the SMX signal group, the groove depth explicit fringes are shifted in the β direction of the pupil for increasing groove depth. This has the effect of masking the overall rotational modulation of the SMX signal group and increasing the net modulation along the β direction of the pupil. The point of minimum rotation in the pupil is for groove depth of $\lambda/6$ and the point of maximum modulation along the β direction of the pupil is for groove depth of $\lambda/8$. The modulation of the IMX signal group is rotational due to the single group of interference fringes. The IMX fringes shift in the pupil for changing groove depth, which determines the amplitude
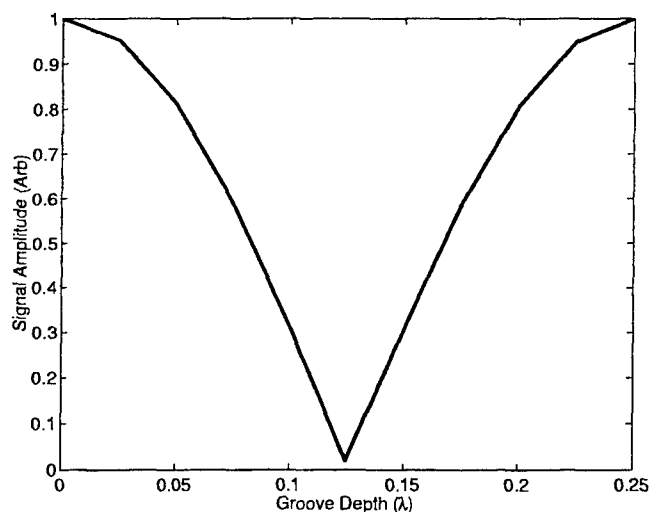
Figure 13. For the IMX signal group. The amplitude of the QPD signal as a function of groove depth. The variation of the QPD signal amplitude with groove depth is due to the positive and negative contributions of irradiance in the pupil.

of the integrated IMX signal. The rotational modulation in the pupil is unaffected by the variation of groove depth because IMX consists of a single set of interference fringes.

REFERENCES

1. T. D. Milster *Conference digest of the optical data storage meeting* **60**, 1997.
2. "Matlab is a registered product of mathworks inc.."
3. D. Flagello, T. D. Milster, and A. E. Rosenbluth, "Theory of high-na imaging in homogeneous thin films," *Journal of the Optical Society of America* **13**(1), 1996.
4. T. D. Milster, "New way to describe diffraction from optical disks," *Appl. Opt.* **37**(29), 1998.
5. H. H. Hopkins, "Diffraction theory of laser read-out systems for optical disks," *Journal of the Optical Society of America* **69**(1), 1979.
6. J. E. Harvey, "Fourier treatment of near-field scalar diffraction theory," *American Journal of Physics* **47**(11), 1979.
7. R. N. Bracewell, *The Fourier Transform and it's Applications*, McGraw-Hill, second ed., 1986.
8. T. D. Milster and R. S. Upton, "Fundamental principles of crosstalk in optical data storage," *Jpn. J. Appl. Phys.* **38** **Part1**(3B), pp. 1608–1613, 1999.
9. G. Bouwhuis, *Principles of optical disk systems*, Adam Hilger, 1986.
10. T. D. Milster, Z. Chen, E. P. Walker, M. T. Tuell, and E. Gage, "Optical data storage readout with quadrant pupil detection," *Appl. Opt.* **35**(14), pp. 2471 – 2476, 1996.
11. R. S. Upton, F. Akhavan, T. D. Milster, W. Bletscher, J. K. Erwin, M. Schweisguth, and A. M. Nichol, "Electronic crosstalk cancellation using a quadrant cell detector," *Jpn. J. Appl. Phys.* **39**(Part 1, No. 2), 2000.
12. C. S. Chung, T. K. Kim, S. T. Jung, C. W. Lee, S. S. Joo, and I. S. Park, "New method of the readout signal generation to reduce the adjacent track crosstalk," *SPIE Conf. Proc. International Symposium on Optical Memory* **3864**, pp. 237 – 239, 1999.